Ann. Geophys., 26, 413–429, 2008
www.ann-geophys.net/26/413/2008/

Annales Geophysicae

Interdependence of tropical cirrus properties and their variability

S. V. Sunilkumar, K. Parameswaran, and Bijoy V. Thampi

Space Physics Laboratory, Vikram Sarabhai Space Centre, Trivandrum-695022, Kerala, India

Received: 12 February 2007 – Revised: 3 December 2007 – Accepted: 19 December 2007 – Published: 26 March 2008

Abstract. The mean properties of tropical cirrus, such as cloud top, cloud base, optic centre, cloud strength/optical depth, asymmetry factor and cloud depolarization, as well as their heterogeneities are examined using lidar observations over 281 nights from a tropical station Gadanki (13.5° N, 79.2° E) during the period 1998–2002. This study shows that as the cloud optical depth (τ_c) increases the cloud becomes more asymmetric in its scattering property. The amount of asymmetry is less than 2% for very low values of τ_c and increases nonlinearly with an increase in τ_c. The physical properties of these clouds also show significant variation with different time scales during the course of each night. On average, while the short-term variations in τ_c are in opposite phase with those of the asymmetry factor (ξ) and volume depolarization ratio (δ), the long-term variation in τ_c extending over a night are found to be in opposite phase with that of ξ and in-phase with that of δ. The short-term variations in δ and τ_c were attributed to possible changes in the cloud particle orientation and the long period variations to cloud evolution process. The value of δ shows a pronounced variation along the vertical, with low values near the cloud top and cloud base and high values in the middle, which is attributed to the cloud dynamics.

Keywords. Atmospheric composition and structure (Cloud physics and chemistry; Transmission and scattering of radiation) – Meteorology and atmospheric dynamics (Tropical meteorology)

1 Introduction

While our knowledge of the characteristics of cirrus clouds, which are seen over about 20–30% of the globe at any time, has improved significantly in recent years, due to long-term observational programs (e.g. Sassen et al., 2001) and several field campaigns (e.g. Starr, 1987; Rashke, 1988), as well as concerted modelling efforts on the part of a few researchers (Starr and Cox, 1985a, b; Jensen et al., 2001a, b), a good deal remains to be learned. Extended ground-based measurements were made by various groups from southern and northern Australia (Platt et al., 1987), the tropical western Pacific region (Platt et al., 1998), Southern Japan (Imasu and Iwaska, 1991), and eastern Great Basin of United States (Sassen and Cho, 1992) to study the geometrical and optical properties of high altitude cirrus. Recent advances in instrumentation have significantly enhanced the capabilities of cirrus cloud research.

Using a ground-based lidar at Kwajalein island (8.7° N, 167.7° E) Uthe and Russell (1977) observed cirrus between 12 and 18 km quite frequently with a geometrical thickness of less than 1 km. Remote sensing observations by satellites (Rossow and Schiffer, 1991; Wang et al., 1996), ground-based lidars (Mather et al., 1998), and airborne lidars (Jensen et al., 1996b; Winker and Trepte, 1998) have revealed the frequent occurrence of thin cirrus layers near the tropical cold-point tropopause at altitudes between 15 and 18 km. Satellite observations have provided global information on the distribution of cirrus clouds and their principal characteristics. These studies revealed the presence of optically thin cirrus very close to the tropical tropopause 50% of the time (Woodbury and McCormick, 1983; Prabhakara et al., 1988; Wang et al., 1994, 1996). Airborne lidar observations of equatorial cirrus acquired during the Central Equatorial Pacific Experiment (CEPEX), the Tropical Ocean Global Atmosphere Coupled Ocean-Atmosphere Response Experiment (TOGA COARE) and the Tropical Ozone Transport Experiment/Vortex Ozone Transport Experiment (TOTE/VOTE) (Jensen et al., 1996b; Heymsfield et al., 1998; McFarquhar et al., 2000; Sassen et al., 2000; Pfister et al., 2001) also revealed frequent occurrences of a geometrically thin cirrus layer very close to the tropical tropopause. Recently, Dessler

Correspondence to: S. V. Sunilkumar
(sv_sunilkumar@vssc.gov.in)

Published by Copernicus Publications on behalf of the European Geosciences Union.

et al. (2006) also reported the presence of thin cirrus near the tropopause region over the tropics using the Geoscience Laser Altimeter System (GLAS), carried on board the ICE, Cloud and land Elevation Satellite (ICESat) and showed that they occur more frequently over the regions of intense convective activity.

Wang et al. (1996) studied the zonal mean distribution and latitudinal variation of high clouds using SAGE II data. They showed that the favoured locations for sub-visual cirrus are centered over southeastern Asia, India and Mexico. The distribution of the zonal mean cloud frequency is consistent with the tropospheric mean circulation (Hadley and Ferrel cells) and longitudinal distributions in the tropics are generally consistent with the cloud pattern associated with the equatorial circulation, including the walker circulation. Studies on high altitude cirrus clouds were also carried out utilizing the data from the Lidar In-space Technology Experiment (LITE) (Winker and Trepte, 1998), the Cryogenic Limb Array Etalon Spectrometer (CLAES) experiment (Mergenthaler et al., 1999), and the Halogen Occultation Experiment (HALOE) (Massie et al., 2000). These studies showed, however, the frequent occurrence of cirrus in maritime environments of Indonesia, Africa and South America primarily during northern winter. The above studies reveal that the occurrence of cirrus at different locations shows distinctly different features. Extensive measurements of SAGE II and High Resolution Infrared Spectrometer (HIRS) showed that the cirrus formation is mostly favoured over the Indian Subcontinent (Wang et al., 1996; Wylie and Menzel, 1999).

The optical thickness of tropical cirrus shows large variability ranging from less than 0.01 to 1. Based on this, the cirrus clouds are classified as thin or dense cirrus. Though the classification based on cloud optical depth (τ_c) is somewhat arbitrary, it is useful for defining different cloud types. Wang et al. (1996) classified cirrus clouds with $\tau_c < 0.03$ as sub-visual clouds and clouds with $\tau_c > 0.03$, as dense clouds based on the measurements from Stratospheric Aerosol and Gas Experiment (SAGE) II extinction profiles at 1-μm wavelength. Guasta et al. (1993) used Ruby lidar (at 0.69 μm wavelength) for cirrus studies. They took a critical τ_c value of 0.05 for sub-visual cirrus and clouds with τ_c above 0.05 as dense cirrus. Several researchers adopted $\tau_c \leq 0.05$ as a threshold for visible optical depth (Lynch, 1993; Schmidt et al., 1993; Schmidt and Lynch, 1995) in identifying sub-visual cirrus. Sassen and Cho (1992) made a detailed classification based on τ_c (at 0.69 μm wavelength) in which clouds with $\tau_c \leq 0.03$ are classified as sub-visual cirrus (SVC), those having $\tau_c > 0.3$ as dense cirrus (DC) and those having τ_c in between the two as thin (bluish coloured) cirrus (TC). The lidar-derived τ_c tends to reach saturation approximately when τ_c reaches about 2–3, in which case the clouds (Kinne et al., 1992) are the dense Cirrostratus (Cs). It may be noted in this context that though the above classification of cirrus is based on τ_c at different wavelengths, the criteria of the fixing threshold τ_c is independent of wavelengths, due to the fact that the cloud optical depth does not show any significant wavelength dependence in the visible region of the electromagnetic spectrum, as the scattering efficiency of the cloud particles lies close to 2 for all wavelengths in this region (Macke et al., 1998). Among the different cirrus classifications cited above, the one proposed by Sassen and Cho (1992) is adopted for the present study because it provides three classes for which τ_c are significantly different and thus provides a finer classification for thin, medium and thick type clouds. McFarquhar et al. (2000) also used a similar classification for cirrus clouds for assessing their radiative impacts.

Due to the ubiquitous nature and higher altitude of the formation, the properties of tropical cirrus are distinctly different from those of the mid-latitude cirrus. Lidar observations from the tropical location, Gadanki (13.5° N, 79.2° E) shows that cirrus clouds occur more than 50% of the time over an year and in most cases they occur in the altitude region around 14–16 km (Sunilkumar et al., 2003). The general properties of tropical cirrus and its association with tropospheric turbulence are reported in the earlier publications (Parameswaran et al., 2003; Sunilkumar et al., 2003) using the data for 195 nights during the period 1998–2001. In this paper we present the interdependence of tropical cirrus properties based on an extended database covering 281 nights during the period 1998–2002.

2 Experimental system and data analysis

The co-located lidar and radar systems at the National Atmospheric Research Laboratory (NARL), Gadanki, near Tirupati, provide an excellent opportunity to study the tropical cirrus clouds and their association with the prevailing tropospheric structure and dynamics. The lidar equipped with a Nd:YAG laser (Model: PL8020, Continuum, USA), emitting linearly polarized pulses at a second harmonic wavelength of 532 nm with a 550-mJ pulse energy, has a laser pulse-width of 7 ns at a repetition rate of 20 Hz with a beam divergence of 0.45 m rad. This beam is further expanded using a 10X beam expander before transmitting vertically into the atmosphere, to reduce the divergence to $<$0.1 m rad. The backscattered photons are received through a 350-mm diameter Schmidt-Cassegrain telescope with a field-of-view of 1-m rad. The lowest altitude from which a usable lidar signal is obtained is $\sim$7 km, limited by the field overlapping of the transmitter and receiver. A narrow band (1.1 nm, FWHM) interference filter is used to suppress the unwanted background. A polarized beam splitter in the receiver beam path splits the beam into a co-polarised (P channel) and a cross-polarised (S channel) component which are detected independently using two identical PMT channels operated in photon counting mode and acquired with a dwell time of 2 μs (corresponding to an altitude resolution of 300 m) over 1024 range bins and summed over 250 s (5000 transmitted pulses) to achieve a good signal-to-noise ratio up to an altitude greater than

30 km. The Mesosphere-Stratosphere-Thermosphere (MST) radar was also operated simultaneously on a few nights along with the lidar to study the temperature structure in the troposphere and lower stratosphere. The technical details of the MST radar system and the method of temperature estimation are described elsewhere (Rao et al., 1995; Revathy et al., 1996).

The method of estimation of backscatter ratio, depolarization ratio and extinction profile from the lidar data is described in detail in an earlier communication (Sunilkumar et al., 2003). The lidar backscattered signals from the P and S channels (co-polarized and cross polarized components, respectively) are analyzed to obtain the altitude profile of the backscatter coefficients (β_p and β_s, respectively) in the altitude region 7–25 km, employing Fernald's method (Fernald, 1984) taking 30 km as the reference altitude where the aerosol contribution is assumed to be negligible. The altitude profile of the molecular backscatter coefficient (β_m) required for the lidar signal inversion is estimated from the mean molecular profile for that month (Sunilkumar et al., 2003), obtained from the model profiles of pressure and temperature (Sasi, 1994) applicable for this region. The lidar signal is calibrated using this mean molecular profile, the maximum uncertainty of which never exceeds 5% (Sunilkumar and Parameswaran, 2005). The molecular backscatter coefficients (β_{mp} and β_{ms}, the co-polarized and cross polarized components, respectively) are estimated from the mean molecular profile, assuming a molecular depolarization factor (δ_m) of 0.028 in accordance with Bodhaine et al. (1999). The backscatter ratios for the co-polarized (R_p) and cross-polarized (R_s) components estimated from the respective backscatter coefficients (β_p, β_{mp} and β_s, β_{ms}, respectively) (Winker and Osborn, 1992) are used to estimate the "unbiased" or (Osborn et al., 1990) effective backscatter ratio (R_e) as

$$R_e(h) = \frac{R_p(h) + \delta_m \; R_s(h)}{1 + \delta_m}. \tag{1}$$

The volume depolarization ratio (δ) and particle depolarization ratio (δ_a) are estimated from the two quadrate-polarized components of the lidar-backscattered signal (Winker and Osborn, 1992; Sakai et al., 2000) as

$$\delta(h) = \delta_m \; \frac{R_s(h)}{R_p(h)} \tag{2}$$

$$\delta_a(h) = \frac{R_p(h)\,\delta(h) - \delta_m}{R_p(h) - 1}. \tag{3}$$

Altitude profiles of backscatter coefficients, backscatter ratios as well as depolarization ratios are estimated from the altitude profiles of lidar backscatter signal taken at every 250 s on different nights. The cirrus cloud is identified in the altitude region 8 to 20 km using a threshold condition for the backscatter ratio to exceed 2 in either of the two channels (i.e. R_p or R_s) and $\delta > 0.04$. On the basis of this, in the cloud detection algorithm the cloud base (h_{cb}) and cloud top (h_{ct}) are identified using the altitude profiles of R_p, R_s and δ. The cloud strength (C_s), cloud mean altitude (h_m) and cloud semi-thickness (Δh) are estimated from the zero, first- and second-order moments of the altitude profile of effective backscatter ratio, as described in Sunilkumar et al. (2003). The first moment of the effective backscatter ratio (R_e) gives the mean altitude (h_m) of the cloud. This is usually referred to as the altitude of the cloud optic centre. If the altitude variation of the scattering property of the cloud is distributed normally (Gaussian distribution), the cloud optic centre will coincide with the geometric centre. The fact that it deviates from the geometric centre indicates that scattering is non-symmetric. If this optic centre is below the geometric centre, it indicates that most of the scattering occurs from the lower part. The amount of this deviation could be stated more quantitatively by examining the asymmetry factor.

Another physical property of the cirrus is its optical depth. For the present case this will be for the visible region of the solar spectrum. The cloud optical depth (τ_c) is defined as the integrated extinction coefficient (α_a) of cloud particles from the cloud base to the cloud top, which can be written as

$$\tau_c = \int_{h_{cb}}^{h_{ct}} \alpha_a(h)\, dh. \tag{4}$$

Based on the optical depth the cirrus clouds are classified as sub-visual cirrus (SVC) with $\tau_c \leq 0.03$, thin cirrus (TC) with $0.03 < \tau_c \leq 0.3$ and dense cirrus (DC) with $\tau_c > 0.3$.

Inversion of the lidar-backscattered signal requires a priori knowledge of the effective lidar ratio for aerosols (S_1) and air molecules (S_2) present in the scattering volume. Though a constant value of $8\pi/3$ could be used for S_2, the range of values reported for S_1 by various investigators varies significantly. While the value of the extinction-to-backscatter ratio derived from ray-tracing simulations (e.g. Sassen et al., 1989) in simple hexagonal ice crystal shapes provided a value of 38 sr for the thin plate, 11.6 sr for the thick plate, and 26.3 sr for the column models, the model calculation of Reichardt et al. (2002) yielded values in the range 5–20 sr for the columnar crystals and those in the range 15–35 sr for the plate-like crystals. Though Sassen and Cho (1992) have used a mean value of 20 sr for cirrus clouds, this was the upper limit reported by Ansmann et al. (1992), employing combined Raman elastic backscatter measurements. While measurements by Whitemann et al. (2004) at Andros Island indicated a steady increase in S_1 from $\sim 16 \pm 10$ at -30°C to $\sim 30 \pm 12$ at -70°C, Seifert et al. (2007) reported a value of $\sim 30 \pm 10$ in most cases, based on measurements at Hulule (4.1° N, 73.3° E), especially during the southwest monsoon period. The major disparity between model and observation could be attributed to the effect of multiple scattering. Platt and Dilley (1981) reported that the multiple scatter correction factor (η) varies from 0.55 to 0.75 as the cloud temperature

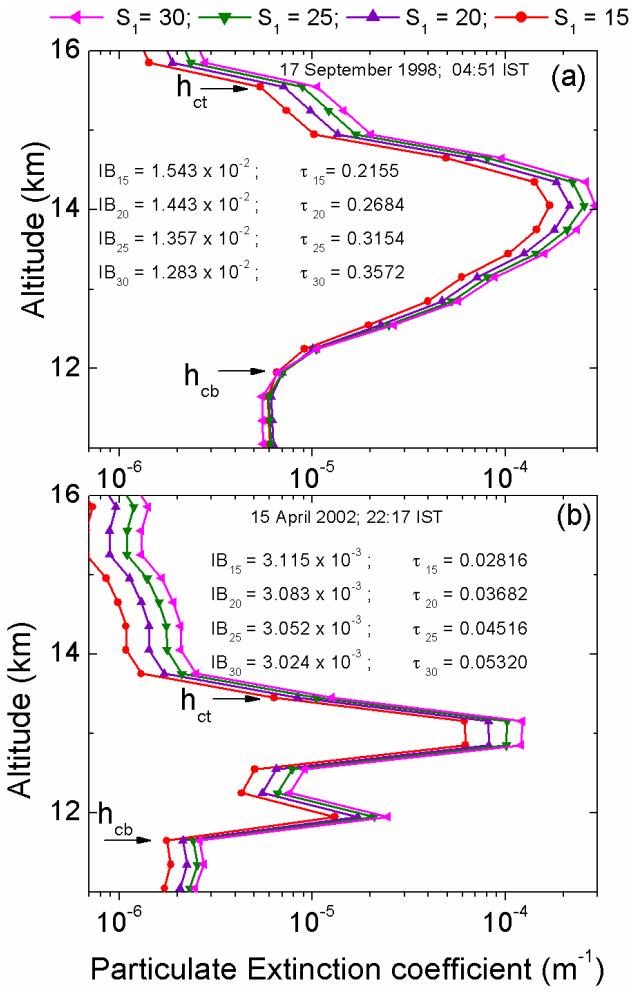

Fig. 1. Altitude profiles of particulate extinction coefficient with thick and thin cirrus for different values of lidar ratio S_1.

increases from −60°C to −20°C with a rapid increase around −40°C. While Sassen and Cho (1992) suggested a value of ∼0.75 as the appropriate value of η for sub-visual and thin cirrus, Platt et al. (1987) suggested a value close to ∼0.4. In the present study, as we are dealing only with semitransparent cirrus (τ_c<1), this effect will be less significant. For temperatures below 240 K (which is the true for the present study) the clouds would contain significant amounts of non-spherical ice crystals of the long column type (Thomas et al., 1990) for which the model quoted value of the extinction-to-backscatter ratio is ∼26.3 (Sassen et al., 1989). Taking a value of 30 for this ratio and a lower limit of 0.55 for η, yields a value of ∼17 for the product of the two, which is the effective lidar ratio (S_1) for cirrus particles. The value of S_1 increases to ∼23 when a value of 0.75 is used for η. Considering the large variability and uncertainty in the reported value of η, an effective value of 20 is used for S_1 in the present analysis which can be considered as appropriate for cirrus (Liu et al., 2000). However, taking note of the uncertainty associated with S_1 a sensitivity analysis is performed to access the possible uncertainties in the derived cloud parameters.

Figure 1 shows the altitude profiles of particulate extinction coefficient (α_a) estimated with four typical values of S_1 (15, 20, 25, 30) for two cirrus cases. In the former case the observed cirrus was thick while in the latter case it was thin. Altitude profiles of α_a obtained are presented in each case. The cloud boundaries estimated using the threshold conditions of the backscatter ratio and volume depolarization ratio are shown with a horizontal arrow head. The cloud boundaries remained same (within the altitude resolution of lidar) for different values of S_1. If we use the backscatter ratio (R_p and R_s) alone as the threshold condition, the cloud boundaries remains the same for all of the above cases except for thick cirrus when S_1 is 15. In this case the cloud base decreases by five bins (1.5 km) in altitude. The estimated cloud optical depths (τ_{15}, τ_{20}, τ_{25}, τ_{30}) for these cases and integrated particulate backscatter coefficients (IB_{15}, IB_{20}, IB_{25}, IB_{30}) within the cloud are listed in the respective frames. This analysis shows that the integrated backscatter coefficient decreases with an increase in S_1, whereas optical depth increases with S_1. It is found that uncertainty introduced in τ_c due to S_1 is large for thin cirrus compared to the corresponding uncertainty in the integrated backscatter coefficient.

For a given uncertainty of 25% in S_1 (=20±5), the maximum uncertainty in aerosol backscatter coefficient (β_a) is 10% in the absence of clouds, ∼15% for thin cirrus and ∼30% for thick cirrus. For the same uncertainty in S_1, the maximum uncertainty in the retrieved backscatter coefficient and R_e are around 0.6%, 2% and 10%, respectively, for clear atmosphere, atmosphere with thin cirrus and atmosphere with thick cirrus. The corresponding uncertainty in the cloud mean altitude is <0.02% for thin cirrus and <0.15% for thick cirrus. Including the possible errors in the lidar signal inversion associated with the uncertainty in the molecular backscatter coefficient, the resultant error in the derived optical depth would be ∼20%. As the signal-to-noise ratio was >2 up to ∼45 km for altitudes <30 km the system-induced errors will be significantly small (<1%) compared to that from other sources (Sunilkumar and Parameswaran, 2005).

3 Results and discussion

Out of 281 nights of observation during the study period cirrus clouds were detected on 217 nights (77.2% cases). However, this statistic is larger than the percentage of cirrus occurrence derived from individual profiles (∼55%), mainly due to the fact that in most of the nights the observed cirrus were either intermittent or occurred only for a short duration during the period of lidar observation. In 63% of the cases the observed cirrus clouds were of the sub-visual (with $\tau_c \leq 0.03$) type and in 30% of cases they were thin cirrus

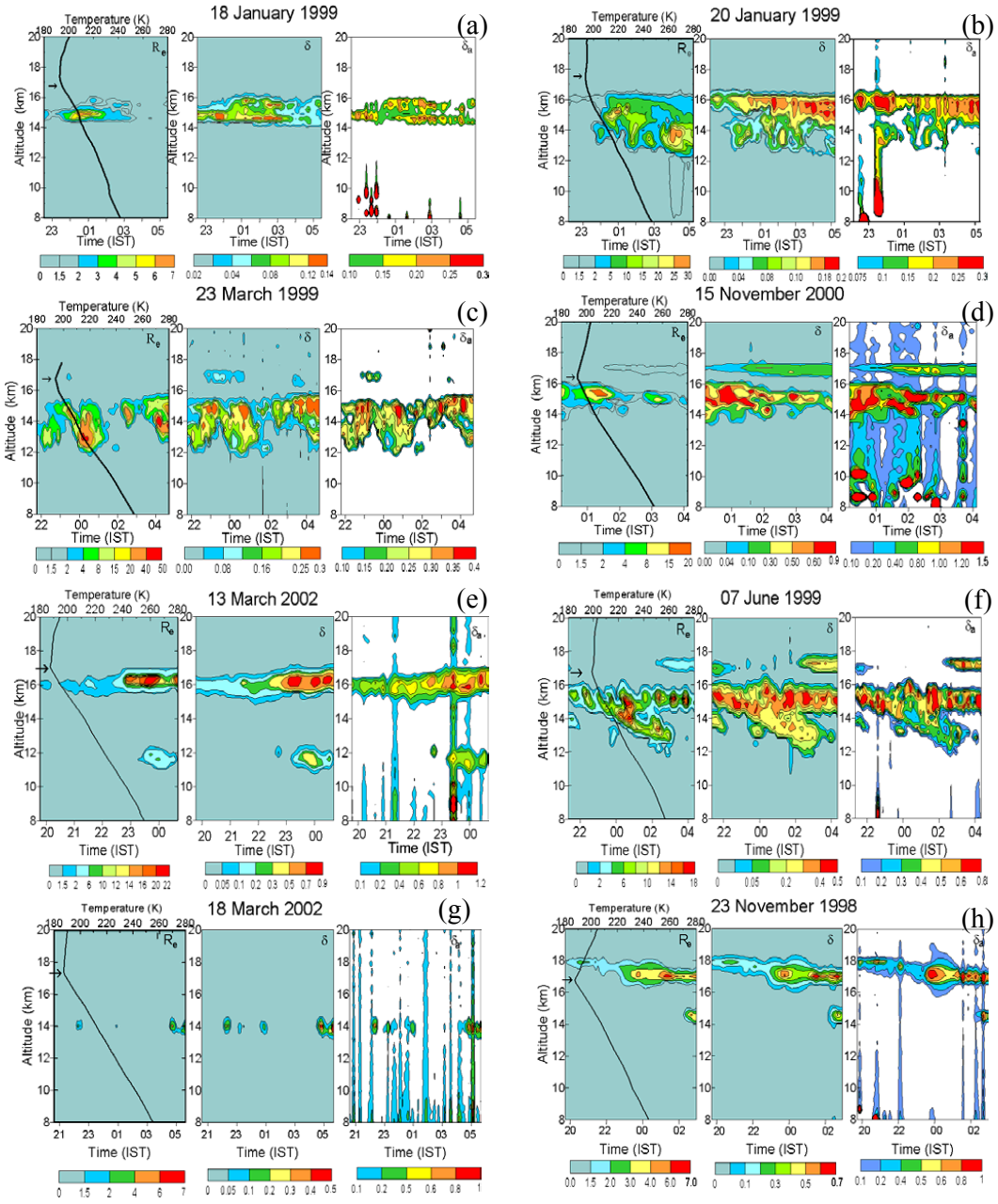

Fig. 2. Different forms of cirrus manifestations observed at the tropical station Gadanki. In each set the first panel shows the contour plot of the effective backscatter ratio (R_e), the middle panel that of volume depolarization ratio (δ) and the end panel that of the particulate depolarization ratio (δ_a). The altitude profile of temperature derived from MST radar data is superposed on the first panel to depict the cold point (tropopause) level.

(with $0.03 < \tau_c \leq 0.3$). In rest of the cases they were dense cirrus (with $\tau_c > 0.3$). Another category of cirrus which falls within the sub-visual range of cirrus, called "ultra thin cirrus" (UTC), with optical depth $<10^{-3}$, is also observed occasionally at this tropical station, most often very close to the cold point. Observations of UTC are also reported by several investigators (Immler et al., 2007; Peter et al., 2003; Luo et al., 2003) from other tropical locations. They reported a vertical extent of 200–300 m for such clouds. However, our lidar does not capture such types of clouds in most cases, due to constraints in range resolution (300 m).

As a perusal of cloud structure showed significant short-term variation during the course of each night, the short-period and long-period oscillations in cirrus properties, such as cloud base, cloud top, cloud optic centre, asymmetry factor, cloud strength/optical depth and cloud depolarization

and their interdependence on each night, are examined separately, and presented in Sect. 3.1. The day-to-day variability in the mean properties of tropical cirrus observed on different nights and their interdependence are presented in Sect. 3.2. It would be worth in this context to note that the cirrus clouds will have a large horizontal extent of a few hundreds of kilometers, as they will also be moving along with the horizontal wind, the temporal variations seen in lidar signature over a night cannot be purely attributed to temporal evolution of cirrus but also could be due to their spatial heterogeneity.

3.1 Short-term temporal variation of cirrus properties and their interdependencies

3.1.1 Manifestations of tropical cirrus

Figure 2 shows the altitude-time contours of the effective backscatter ratio (R_e), volume depolarization ratio (δ) and particulate depolarization ratio (δ_a) for different nights depicting the distinct nature of cirrus structures. The mean temperature profile derived from the vertical wind data of the MST radar (for a period of 2 h from 22:00 IST to 24:00 IST) is superposed along the corresponding contours of R_e for that night. The cold point tropopause identified from temperature profiles is indicated by an arrow mark. As can be seen from this figure the contour of δ is a good indicator for the region where the cloud is present. As the backscatter ratio is small at cloud boundaries (especially at its base) the altitude extent of the cloud will not be fully represented by its contour. However, the region in which the cloud is very strong (in terms of its backscatter) could be seen clearly from the contour of R_e. Though the particulate depolarization ratio also reveals the structure of cloud boundaries, in some cases, due to the possible non-sphericity associated with aerosol particles above and below the cloud, values of δ_a could be larger beyond the cloud boundaries, in which case the contour of δ would be a better indicator for depicting the cloud.

Cirrus observed on different nights revealed distinctly different cloud structure/pattern. Out of 217 nights of cirrus occurrence, single layer formations are observed on 160 nights (74% of observational nights). These single layer formations could either be thin or thick. Thick cirrus are mostly found to be highly structured. A typical example of a single layer thin (laminar) cirrus is shown in Fig. 2a. Figure 2b shows a typical manifestation of a single layer but highly structured dense cirrus. Generally, they occur below the cold point but very close to it. In a very few cases cirrus top penetrates the cold point and intrudes into the lower stratosphere. Figure 2h shows one such rare event observed on 23 November 1998 in which the cloud formation is seen clearly above the tropopause temperature inversion and it persisted in the same region throughout the period of lidar observation. Note that the depolarization ratio is also quite large for this cloud.

For the remaining 26% of observational nights more than one cirrus cloud separated by a clear region (where the backscatter ratio is less than its threshold value and $\delta<0.04$) persists for a significant duration (typically >1 h). Such clouds are referred to as multi-layer cirrus, a typical example of which is presented in Fig. 2e. In this case the two cloud layers are clearly separated by a distance of $\sim$3 km. Some of these clouds could be highly structured dense cirrus topped by a thin cirrus with a very small separation of $\sim$0.6–1 km. Typical examples of such clouds are presented in Fig. 2c, d and f. The occurrence of thin cirrus very close to the tropopause plays a major role in dehydrating the air entering the lower stratosphere (Jensen et al, 1996a). Radiative impact of these clouds on the Earth-atmosphere system will also be quite significant. They can induce local heating by absorbing upwelling long wave radiation near the cold tropopause, which is suggested (Wang et al., 1996; Rosenfield et al., 1998; McFarquhar et al., 2000) to be responsible for producing heating rates of the order of a few K per day. This absorbed radiative energy drives lifting (Gage et al., 1991) of the cloud (the vertical wind speed $\sim$0.2 m/s) which may also persist for longer duration (Jensen et al., 1996b).

Based on the data from 532 nm channel of LITE, Winker and Trepte (1998) observed thin cirrus above the tropical tropopause. Different possible mechanisms are suggestive for the formation of such thin cirrus above the tropopause. Fujita (1982) attributed the observed lower stratospheric cloud near the top of the severe thunderstorms to the violent collapse of overshooting thunderstorm turrets. The flux of air across the tropical tropopause may be dominated by sporadic mass injections associated with overshooting convective cloud turrets that penetrate into the lower stratosphere (Robinson, 1980). Thin cirrus above the tropopause, shown in Fig. 2c, d and f, thus could be due to convective pumping of water vapour and aerosols across the tropopause or the remnants of the thick cirrus. Similar multi-layer manifestation of cirrus was reported by many other investigators over the tropics (McFarquhar et al., 2000; Comstock et al., 2002), sub-tropics (Cadel et al., 2003) and mid latitudes (Goldfarb et al., 2001; Sassen et al., 2001). Satellite and aircraft measurements also showed the presence of thin cirrus above the thick structured cirrus (Winker and Trepte, 1998; McFarquhar et al., 2000; Santacesaria et al., 2003; Thomas et al., 2002).

In the above, we have presented typical cases in which the observed cirrus clouds were strong and persistent almost throughout the duration of lidar observation. But on some nights, the observed cirrus was weak and intermittent in their appearance. In such cases the patches of cirrus appear and disappear at the same altitude on a number of occasions. A typical example of such intermittent cirrus encountered on 18 March 2002 is presented in Fig. 2g. Note that this intermittency in cirrus appearance is not caused by blocking due to the presence of a low level cloud, because in all these cases a strong lidar signal was observed throughout the observation period up to the highest altitude (>30 km) and no indication of low level cloud was observable in this signal. Such intermittent cirrus clouds with a single layer structure

are observed in ∼7% of the nights on which lidar observations are made.

Based on the above typical examples and the information gathered from a perusal of cloud structures on different nights it can be inferred that the tropical cirrus manifestation can be broadly classified into two types; a) thin cirrus and b) dense and highly structured cirrus. Most frequently, they are observed very close to the cold point tropopause. Several observations from satellite, lidar and aircraft have shown the presence of persistent, thin sheets of cirrus clouds very close to the tropopause (Jensen et al., 1996b; Wang et al., 1996; Prabhakara et al., 1988; Comstock et al., 2002). Such thin cirrus clouds which are very frequently observed at this tropical station are usually referred to as laminar cirrus (Winker and Trepte, 1998), based on their physical appearance.

3.1.2 Cloud depolarization

Cirrus clouds, especially over the tropics, are mostly composed of non-spherical ice crystals. These particles will cause significant depolarization to backscattered radiation. Hence the depolarization ratio within the cloud is an indicator of the cloud microphysical properties. Its variation with time and altitude depicts the corresponding variation in particle habit and size. Figure 2 show that generally low values of δ (and δ_a) are encountered near the cloud top and cloud base, and high values are in the middle portion of the cloud. The vertical variation of δ (or δ_a) could be attributed to the changes in the cloud microphysical property associated with cloud formation, growth and decay. In general, the cloud ice water content will be maximum in the middle portion and decreases towards the cloud peripheries (Mace et al., 1998). The altitude profile of cloud microphysical data obtained during FIRE (I and II) indicates that the average ice crystal size increases from cloud top downward up to the cloud base, where it decreases abruptly.

According to the conceptual view of the formation and development of cirrus clouds suggested by Heymsfield and MacFarquhar (2002), based on their observations, the in-situ generated cirrus clouds can be represented by three distinct layers in the vertical: the nucleation layer, the growth layer and the sublimation layer. The upper most part of the cloud, composed of small ice crystals, is called the "nucleation layer", where the relative humidity is more than that required for ice initialization, leading to the formation of small ice crystals. In the middle part of the cloud, called the "growth layer", which is rather thick, the ice supersaturation sustains crystal growth and hence is composed of pristine ice crystals. In the "sublimation layer" near the cloud base, the ice subsaturation causes crystals to sublimate and disappear. This layer is relatively thin and composed of relatively small rounded crystals of a nondescript shape. From the above it can be seen that ice crystals in the nucleation and sublimation layers are either smaller in size or having a lesser non-sphericity compared to those in the growth layer, having larger and highly non-spherical crystals with sharp edges. The depolarization caused by the smaller type crystals (and more-spherical ones having rounded edges) will be smaller than that caused by the larger crystals having sharp edges. This is generally in agreement with the observed feature in the present investigation.

The values of δ varies from 0.03 to 0.9. While on some nights the maximum value of δ encountered is $<$0.2, on some other nights it goes up to 0.9. Similarly values of δ_a, which are relatively larger than those of δ, also show significant variation. The contours of δ_a show interesting features on 15 November 2000. Pockets of high δ_a exceeding unity are observed in the lower cloud layer, which is thick and highly structured. The value of δ within the cloud is also significantly large. Such a large value of δ_a exceeding unity was also reported by McNeil and Carswell (1975). They attributed this to some preferred re-orientation of the electric vector of the polarized backscattered signal, which could be encountered in scattering from an anisotropic layer of preferentially oriented particles resulting from wind shear or due to some other alignment processes prevailing in the atmosphere. More discussion on the dependence of depolarization on ambient temperature (and on altitude) is presented in Sect. 3.2.

3.1.3 Temporal variations of cirrus properties

Temporal variation of tropical cirrus properties are examined for those nights in which single layer cirrus persisted throughout the period of lidar observation (typically 7 to 8 h). Figure 3 shows the temporal variation of cloud base, cloud top and cloud optic centre, along with that of cloud optical depth (τ_c) and cloud strength (C_s) for three typical cases. On 18 January 1999, the observed cirrus was thin while on 20 January 1999 and 23 March 1999 they were rather thick. The altitude of the cold point tropopause identified from the temperature profile is indicated by the arrow mark. A perusal of this figure shows that the temporal variation of the cloud top is relatively small (it remains more or less aligned to the tropopause) while that of the cloud base is quite significant. The cloud optic centre also shows significant variations. On 20 January 1999, during the post-midnight period when the cloud becomes dense, the optic centre descends much below the geometric centre, indicating that much of the scattering occurred from the lower half of the cirrus. Large variations observed in the altitude of the cloud base could be attributed to corresponding variations in strength of the convective turbulence below the cloud. Parameswaran et al. (2003) have shown that turbulence plays a significant role in governing the cloud shape. However, for those high altitude thin cirrus forming just below the tropical tropopause, the temporal variation in cloud top and cloud base is relatively small, a typical example of which is observable in Fig. 3a.

While on some nights the cloud optical depth is very low and they persist as a sub-visual type throughout the night

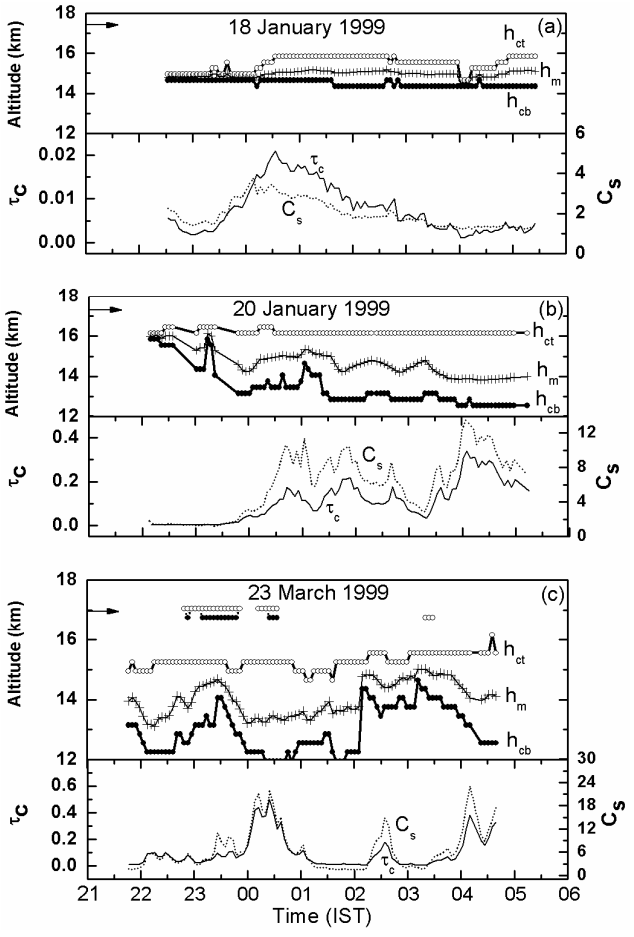

Fig. 3. Short-term variations of cloud top (h_{ct}), cloud base (h_{cb}) and optic centre (h_m) (mean altitude) over a night along with cloud strength (C_s) and optical depth (τ_c) for three typical nights (18 January 1999, 20 January 1999, 23 March 1999).

with a very little variation with time, on other nights the cloud optical depth shows significant temporal variations. The cloud changes from its sub-visual category to thin and even to dense cirrus. Typical examples for both these cases are observable in Fig. 3. Although the optical depth (τ_c) is low on 18 January, for example, the variations in this quantity are appreciable in line with the cloud strength. On 20 January 1999 and 23 March 1999, the variation in τ_c is very large and the cloud type fluctuates between the three classes within a short duration. Figure 3c shows a typical example of optically thin cirrus (with $\tau_c \leq 0.3$) with a larger cloud depth (compared to that in Fig. 3b). On this night also, the cloud which was of sub-visual type in the beginning changed to thin cirrus and subsequently to dense cirrus just after midnight. After this, though the cloud depth remained almost the same, τ_c decreased drastically and the cloud type changed to sub-visual. Around 02:30 IST, even though the cloud depth decreases, the cloud optical depth increased to ∼0.2. This shows that even when the cloud thickness remains fairly constant the cloud optical depth changes significantly. This could be due to the cellular structure of the cirrus (Platt, 1973). Note that in both cases the temporal variation of cloud top was rather small, and the variation in cloud thickness is mainly governed by corresponding variations in the cloud base. Another interesting feature observed on the night of 23 March 1999 is the manifestation of a very weak and geometrically thin cloud strata with $\tau_c < 0.002$ aligned to the cold point tropopause. This could be of a UTC type which persisted only for a shorter duration. Of the 160 nights having a single layer cirrus, the cloud continues to persist in the same category in 47% of the cases (sub-visual type in 39%, dense type in 6% and thin in 2% of the cases) and changes from one type to the other in the remaining 53% of the cases (to be more precise 32% cases from SVC to TC, in 8% cases TC to DC and in 13% cases from SVC to TC and DC).

As seen from Fig. 3, the variation in cloud strength (C_s) and τ_c are well correlated. However, this is quite expected because C_s is the weighted mean backscatter ratio and τ_c is the integrated extinction, both representing the scattering property of the cloud where the absorption is negligible. Such short-term fluctuations in τ_c are also reported by several other investigators (Jensen et al., 1996b; McFarquhar et al., 2000), both over the tropics as well as over the mid-latitude region.

On examining the contour plots presented in Fig. 2a–h, it is seen that the cloud backscatter ratio varies significantly in altitude with high values in the middle and low values towards the peripheries. Note that the altitude of the peak backscatter ratio does not coincide with the geometric centre of the cloud. In other words, as far as scattering is concerned, the cloud is neither homogeneous nor optically symmetric with respect to its centre. The amount of deviation from the symmetric nature could be quantified in terms of the asymmetry factor ξ, defined (Sassen and Cho, 1992) as

$$\xi = \frac{h_m - h_{cb}}{h_{ct} - h_{cb}}. \quad (5)$$

If the altitude profile of the backscatter ratio within the cloud is Gaussian (symmetric with respect to its mean position), ξ will be close to 0.5. A value of ξ less than 0.5 indicates that more scattering occurs from the lower half of the cloud and vice versa. As seen in Sect. 2 and Fig. 1, for a ±25% deviation in S_1 about its mean value of 20, the deviation in h_m is ±0.0026 km for thin cirrus and ±0.02 km for thick cirrus. As the cloud is detected using the threshold condition for the backscatter ratio, along with that of the volume depolarization ratio ($\delta \geq 0.04$) there is no change in the values of h_{ct} and h_{cb}. Then the standard error in ξ, given by $\sigma_\xi = \sigma_{hm}/(h_{ct} - h_{cb})$, is <0.2% for thin cirrus and <1% for thick cirrus.

The short-term variation in ξ is studied by examining its temporal structure with a resolution of 4 min on different nights. Figure 4a–c shows the variation of ξ for 18 January 1999, 20 January 1999 and 23 March 1999, respectively.

On 18 January 1999, at the start and at the end of the lidar observation, the value of ξ is close to 0.5, indicating that the backscatter ratio distribution in the cloud is more or less Gaussian and the optic centre of the cloud coincides with the geometric centre. But during midnight and in the post-midnight period, ξ decreases significantly from 0.5 reaching as low as 0.38 around 00:30 IST, which indicates that the cloud optic centre has shifted below its geometric centre. Also on 20 January 1999 and 23 March 1999, ξ shows significant temporal variations. These typical samples show that the short-term variation of ξ is distinctly different on different nights.

3.1.4 Interdependence of cirrus properties

As seen above, the temporal variation of cloud parameters, as well as the depolarization ratio over a night is mainly composed of a short period fluctuation with a period of tens of minutes (referred to as "short-term" hereafter), superposed on a relatively "long-period" variation (referred to as "long-term" hereafter) extending over the entire night. To quantify the depolarization of the entire cloud ensemble, an effective value of $\delta_i(t)$ at any particular time t is estimated by integrating the altitude profile of $\delta(h,t)$ within the cloud from h_{cb} to h_{ct} and normalizing it to the cloud geometrical thickness, which can be written as

$$\delta_i(t) = \frac{1}{h_{ct} - h_{cb}} \int_{h_{cb}}^{h_{ct}} \delta(h,\ t)\, dh, \tag{6}$$

where $\delta_i(t)$ represents the height averaged values of δ along the cloud thickness. Similarly the effective value of δ_a is also obtained and is denoted by δ_{ai}.

Figure 5a–f shows the temporal variation of ξ, τ_c, δ_i and δ_{ai} for a few typical nights in which they showed distinct features. They show significant variations with a period of a few minutes to a few hours. While on some nights ($\sim$47%), even though τ_c shows significant temporal variation, the cloud type remains the same; on other nights the variation in τ_c is so large that the cloud type changes from one class (SVC/TC/DC) to the other at short time scales. The weighted mean values of δ and δ_a (δ_i and δ_{ai}) also shows significant temporal variations, which are more-or-less similar in nature (though short-term variations are more pronounced in δ_{ai}). Because of this we deal only with the temporal variation of δ_i in studying the interdependencies, along with the other cirrus properties. In general, as cloud optical depth increases ξ decreases. Correspondingly, the depolarization ratio shows an increase, indicating that cloud particles tend to become more non-spherical in nature. On a long-term basis the variation of ξ and τ_c are in opposite phase while that of δ_i and τ_c are in-phase. These features are clearly observable in Fig. 5c and d on the nights of 18 January 1999 and 16 November 2000, respectively. However, the integrated volume depolarization ratio (δ_i), shown in the lower panel

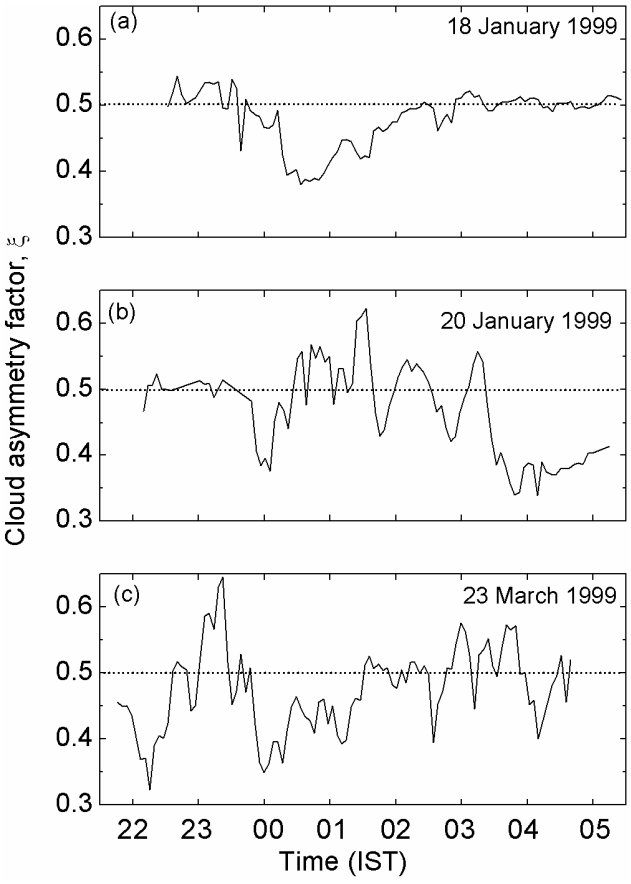

Fig. 4. Temporal variation of cloud asymmetry factor (ξ) observed on three different nights in the year 1999 as typical examples.

of Fig. 5c (18 January 1999), on average, remains more or less steady (with short-term fluctuations) around 0.08 up to 03:00 IST, followed by a sharp decrease to a value less than 0.05 when the cloud optical depth decreased to $<$0.005. On a few other nights, the long-term variation of τ_c is found to be in-phase with that of both ξ and δ_i. One such example is shown in Fig. 5b. On 8 May 1998 the long-term variations of τ_c and ξ are in opposite phase up to 02:00 IST. But subsequently in the last two hours of observation these variations became in-phase.

In addition to these long-term variations, τ_c, ξ and δ_i also show significant short-term variations during the course of each night. On the majority of the nights the short-term variations in τ_c are found to be in opposite phase with that of ξ and δ_i. However, on a few nights the short-term variation of δ_i and τ_c are found to be in-phase (e.g. Fig. 5b and c). Figure 5e and f shows two typical examples in which ξ and τ_c shows significant short-term fluctuations compared to the long-term variations. While in most of the cases the long-term variation in δ_i and τ_c is found to be in-phase, the short-term variation are out-of-phase. The short-term variation in δ_i and τ_c could be attributed to the changes in the orientation

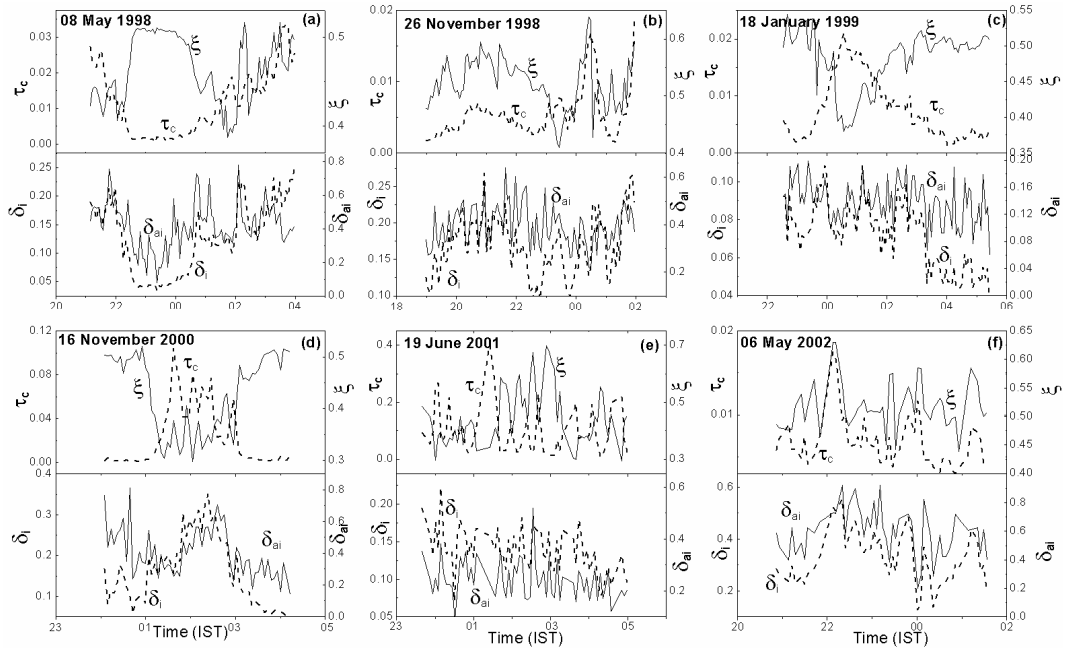

Fig. 5. Temporal variations of cloud asymmetry factor (ξ), cloud optical depth, volume depolarization (δ_i) and particulate depolarization (δai) of the cloud on different nights showing distinct features.

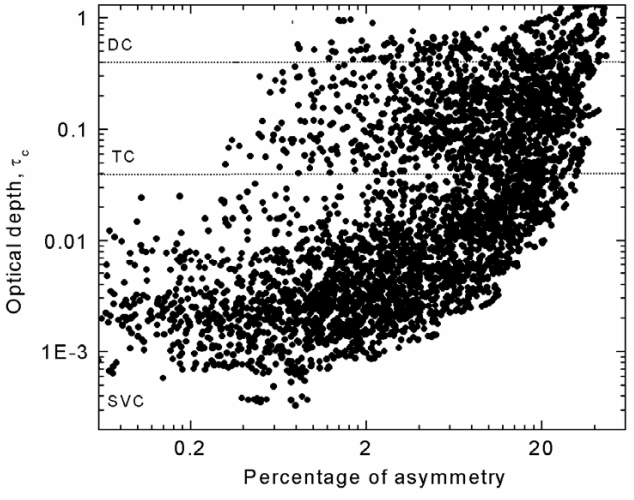

Fig. 6. A scatter plot showing the variation of percentage asymmetry of tropical cirrus with corresponding variations in cloud optical depth (τ_c) from individual profiles on different nights.

of ice crystal, while the longer period variation in δ_i and τ_c could be associated with the formation, development and decay phases of the cloud.

The long-term variations in ξ and τ_c are not always phase consistent. While on some nights, as τ_c increases, the asymmetry factor (ξ) decreases or goes below 0.5, and on some other nights it increases or goes above 0.5. In any case, as the optical depth increases, the cloud becomes more asymmetric. The amount of asymmetry could then be quantified in terms of its absolute deviation from 0.5. The short-term temporal variations are smoothed out by subjecting the time series of ξ and τ_c to a moving average filter of 30 min. The percentage asymmetry is then estimated as $\{|\xi-0.5|/0.5\}\times 100$ and its dependence on τ_c is examined by making a scatter plot, which is presented in Fig. 6. In this figure corresponding parameters are plotted with a time resolution of 250 s for 80 nights, in which continuous observations were available for more than 4 h. This plot shows that for low values of τ_c (<0.01) the asymmetry is less than 2% and increases nonlinearly with an increase in τ_c, indicating that most of the sub-visual cirrus are symmetric. Studies conducted at Mahe Island (4.4° S, 55.3° E) also showed (Pace et al., 2003) that in most of the cases the observed cirrus is symmetric. They attributed the low values of ξ mainly to ice precipitation, leading to the accumulation of ice mass near the cloud base. This condition mostly occurs near the dissipating stage of the cirrus lifecycle when sedimentation processes are more intense. High values of ξ are attributed to ice clouds in the early phases of their evolution, when the larger amounts of ice crystals will be present in the upper part (where the nucleation is initiated because of lower temperature). However, this hypothesis does not match with the present finding where low and high values of ξ are observed when the cloud is strong (τ_c maximum) and tending to 0.5 when the cloud becomes weak (low τ_c).

The short period variations in cirrus cloud parameters (Figs. 3 and 4) could be linked to the dynamical process

that plays a leading role in determining the cloud structure, which includes cells, turbulence, eddies and waves (Gultepe and Starr, 1995; Gultepe et al., 1995). Turbulence occurs intermittently in patches and coexists with wavy motions on a variety of scales. The gravity wave phenomenon is often present within the cirrus systems and potentially influences cirrus processes and hence their physical properties. Boehm and Verlinde (2000) showed a close association between the upper tropospheric cirrus and large-scale dynamics. The radiosonde data revealed the presence of Kelvin waves with downward phase propagation from the lower stratosphere into the upper troposphere. These waves also can modulate the cirrus clouds. The above studies show the necessity of understanding tropical waves and other sources of large-scale rising motion in the upper troposphere, to interpret the observed temporal variation in cirrus properties caused by the interaction of these waves. This involves a detailed study for delineating the dynamical features including wave perturbations in the upper troposphere and relate them to the observed short period (of the order of a few minutes to a few hours) variation in cloud structure which could be addressed at a later stage.

3.2 Mean properties of cirrus clouds in different nights and their interdependencies

From the value of cloud top (h_{ct}) and cloud base (h_{cb}) estimated from individual lidar profiles, the mean value for each night is estimated. The frequency distributions of this (in steps of 0.5 km) for different nights during the period 1998–2002 are presented in Fig. 7. This shows that the frequency distribution of cloud top is rather sharp compared to that of the cloud base. Though cloud top can generally lie between 9 and 20 km, in most of the cases it occurs around 15 to 18 km, very close to the cold point tropopause. Similarly, though the cloud base generally lies between 8 and 18 km, in most of the cases it occurs around 13 to 16 km. The most probable value of cloud top is 16 km and that of cloud base is 14 km, leading to a most probable value of ∼2 km for the cloud depth.

The mean cloud parameters, such as cloud strength (C_s), cloud mean altitude or optic centre of cloud (h_m), cloud semi-thickness (Δh), cloud asymmetry factor (ξ), cloud optical depth (τ_c) and the depolarization ratio (δ_i and δ_{ai}), are obtained by averaging the respective parameters obtained from each lidar profile (with a basic time resolution of 250 s) for individual nights. The frequency distributions of these parameters were presented in an earlier publication (Sunilkumar et al., 2003). It may be noted that, as discussed in Sect. 3.1, these parameters do show some temporal variations during the course of a single night which are not considered in the present discussions, as they pertained only to the mean cloud property over each night.

Figure 8 show plots of τ_c against C_s and Δh, the two parameters governing the cloud optical depth. A significant scattering of points is observed in Fig. 8a, indicating that it

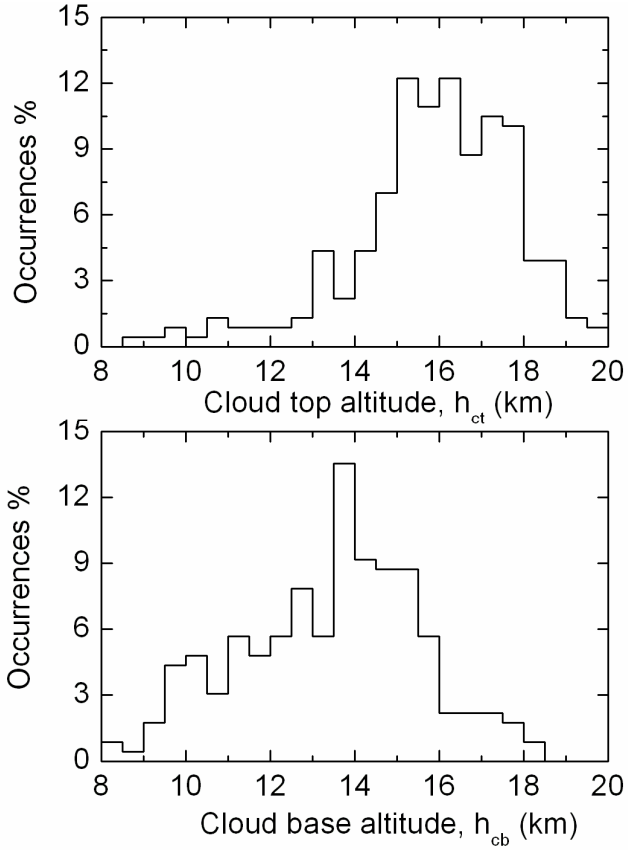

Fig. 7. Observed mean frequency distribution of the cloud top (h_{ct}) and cloud base (h_{cb}) for tropical cirrus at Gadanki for the period 1998–2002.

will be possible to have more than one value for C_s for the same value of τ_c. For sub-visual cirrus with $\tau_c \leq 0.03$, C_s is generally less than 4 and primarily lies in the range 1 to 2.5, while for thin cirrus, for which τ_c lies between 0.03 and 0.3, the value of C_s generally lies in the range 2 to 14, with a highest frequency of occurrence of ∼6±2 for C_s. Both sub-visual and thin cirrus can have cloud strength in the range 2 to 6, but in the majority of such cases they will be thin. Similarly, for dense cirrus ($\tau_c > 0.3$), the value of C_s generally ranges from 6 to 18 and dense cirrus with $C_s < 6$ seldom occur. A simple linear relationship sought between τ_c and C_s is shown in Fig. 8a. Even though a similar relationship can also be seen for Δh and τ_c in Fig. 8b, the standard deviations are significantly large. A similar relation between cloud optical depth and geometrical depth (physical depth) has been reported by various other investigators for tropical cirrus (Pace et al., 2003; Thomas et al., 2002) and mid-latitude cirrus (Sassen and Cho, 1992).

Figures 9, 10 and 11 show the interdependencies of various cloud parameters. In these figures the open circles represent the relevant parameters for sub-visual cirrus, grey and black shaded circles represent those for thin cirrus and dense

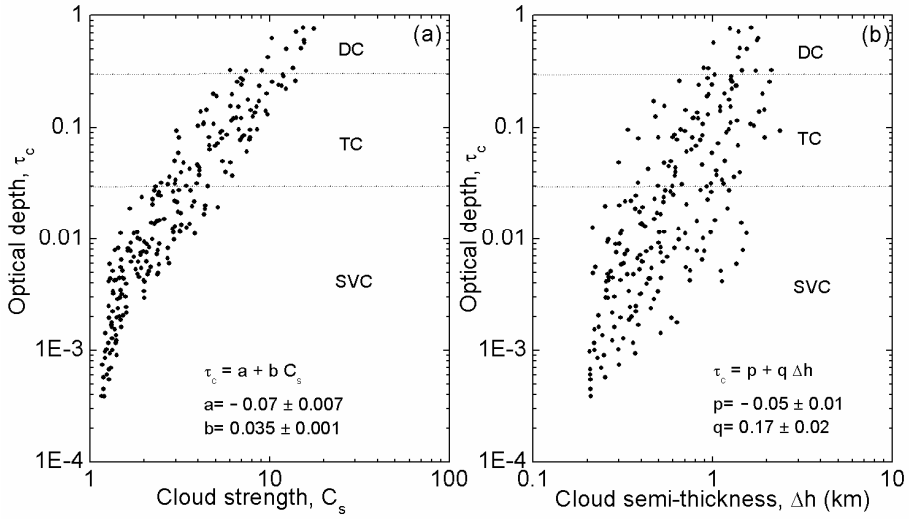

Fig. 8. Scatter plots showing the dependence of cloud optical depth (τ_c) on cloud strength (C_s) and cloud semi-thickness (Δh).

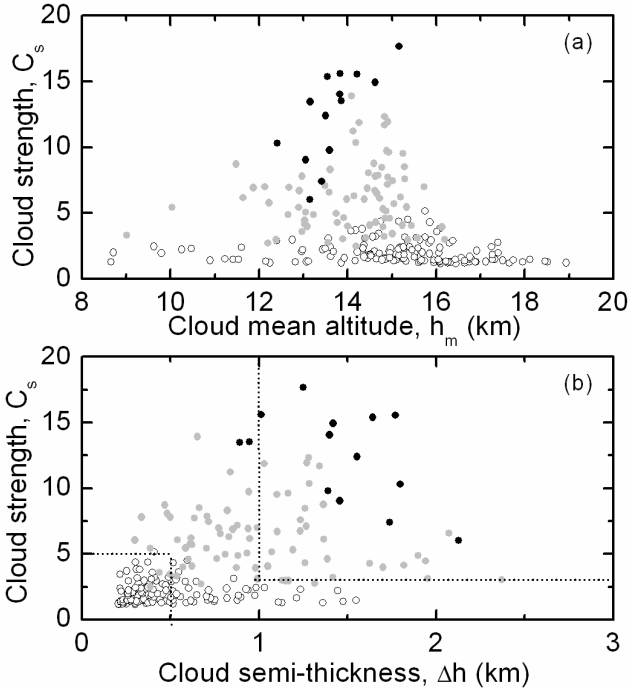

Fig. 9. Scatter plots showing the dependence of mean cloud strength (C_s) on cloud mean altitude (h_m) and cloud semi-thickness (Δh) for tropical cirrus.

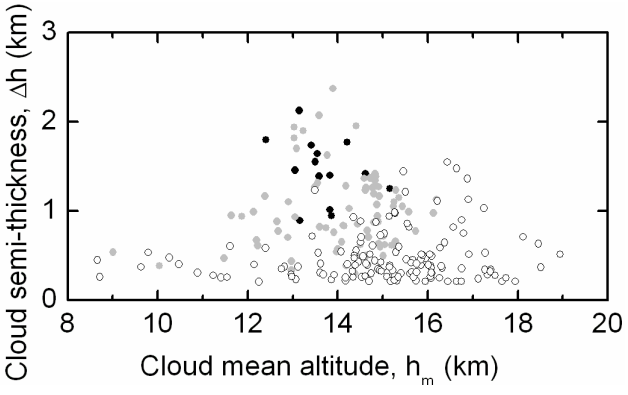

Fig. 10. Scatter plots showing the interdependence of cloud mean altitude (h_m) and cloud semi-thickness (Δh) for tropical cirrus.

cirrus, respectively. Figure 9 shows the dependence of cloud strength on cloud mean altitude and cloud semi-thickness. The mean altitude varies in the range 8 to 20 km, and weak clouds (optically thin clouds with $C_s < 5$) can occur anywhere in this altitude region. But strong clouds with $C_s > 10$ generally occur between 13 and 15 km. Figure 9b shows that thin clouds with semi-thickness < 0.5 km are generally weak with $C_s < 5$ (region marked with small dashed-square). But thick clouds ($\Delta h > 1$ km) are generally strong with $3 < C_s < 20$ (region embedded by the large dashed-square).

A scatter plot of cloud semi-thickness with cloud mean altitude shown in Fig. 10 reveals that cirrus clouds occurring at very low and very high altitudes are generally thin. Thick clouds with semi-thickness > 1 km primarily occur between 13 and 17 km, even though all cirrus clouds occurring in this altitude range need not be thick. High values for Δh are encountered for those clouds with mean altitude $\sim$14 km and these clouds are mostly strong (high values of C_s). It would be worth in this context to note that, as revealed by Fig. 7, this is the most favoured altitude for the formation of tropical cirrus.

Figure 11 shows the scatter plots of the cloud asymmetry factor with cloud strength (top panel), cloud mean altitude (middle panel) and cloud semi-thickness (bottom panel). The

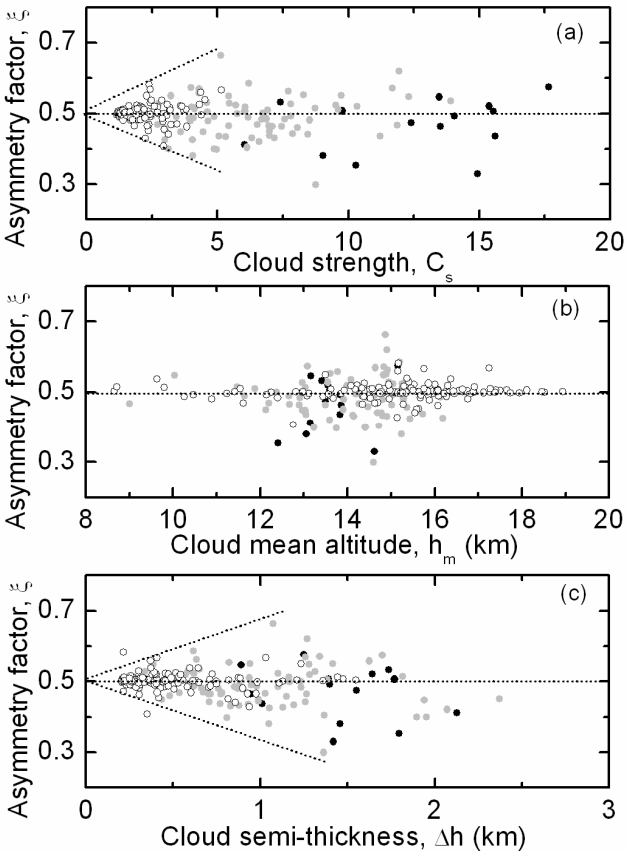

Fig. 11. Scatter plots showing the dependence of cloud asymmetry factor (ξ) on cloud strength (C_s), cloud mean altitude (h_m) and cloud semi-thickness (Δh) for tropical cirrus.

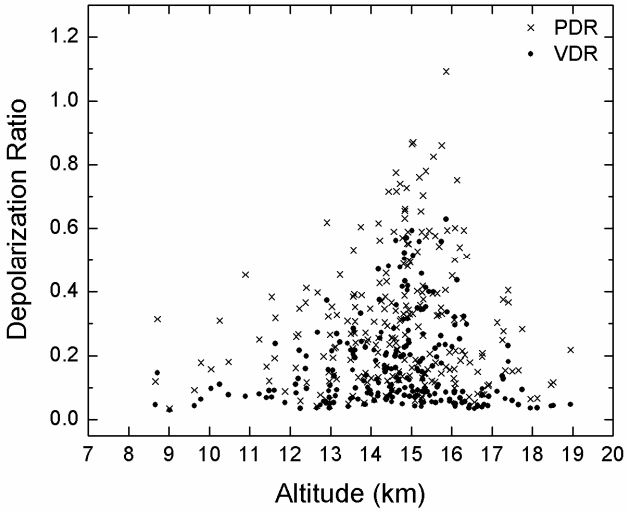

Fig. 12. Scatter plot showing the altitude dependence of volume depolarization ratio (VDR) and particulate depolarization ratio (PDR) of tropical cirrus averaged for individual nights.

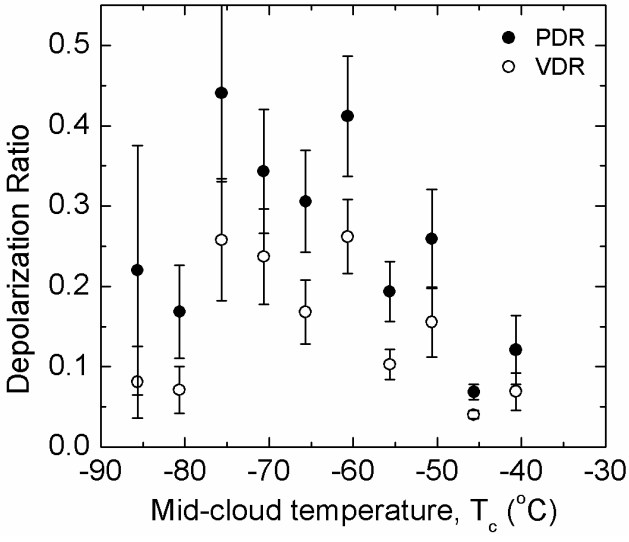

Fig. 13. Temperature dependence of volume depolarization ratio (VDR) and particulate depolarization ratio (PDR). Open circles present the averaged values of VDR and filled circles present the averaged values of PDR grouped at 5°C interval. The vertical bars indicate the associated standard error.

horizontal line in these plots is drawn at ξ=0.5, corresponding to symmetric clouds. The cloud mean altitude (optic centre) is more or less close to the geometrical centre (with $\xi \approx 0.5$) for weak clouds ($C_s < 3$). As the value of C_s increases the clouds becomes more asymmetric, even though quite a few clouds with high C_s values continues to be symmetric. In most of the cases the optic centre of the strong clouds significantly descends from the geometric centre (indicated by a high occurrence of ξ with values much less than 0.5). Note that high and low altitude cirrus are more or less symmetric and significant asymmetry is observed only for clouds forming in the altitude region 12–16 km. Plots in the lower panel show that thin clouds (with low Δh values) are more or less symmetric and the asymmetry increases with increases in Δh. In the majority of cases the optic centre descends from geometric centre ($\xi < 0.5$).

Figure 12 shows the scatter plot of the mean values of the volume depolarization ratio (VDR) and particulate depolarization ratio (PDR) with cloud mean altitude. Although those clouds forming around 14–16 km show both high and low values of depolarization, the clouds forming at lower and higher altitude show low values (<0.2). To study the temperature dependence of cloud depolarization, values of VDR and PDR are grouped at cloud temperature (T_c) intervals of 5°C and then averaged. The variation in these mean values of VDR and PDR with T_c is presented in Fig. 13. Both VDR and PDR generally show a decreasing trend with increase in T_c for values exceeding −75°C. The values of VDR for the temperature range −75°C to −50°C compares favorably with those reported by Platt et al. (1998) for tropical cirrus. However, the mean VDR (also PDR) shows a dip when T_c

decreases below −75°C. Pace et al. (2003) also observed a similar feature from the ground-based lidar data at Mahe (4.4° S, 55.3° E). They have shown that the integrated depolarization values ranges between 0.27 and 0.19 for the temperatures in the range −73°C and −33°C. The tropical cirrus data during the TOGA/COARE campaign also showed a regular increase in δ with a decrease in temperature (from 0.375 at −35°C to 0.5 at −85°C) (Sassen et al., 2000).

The change in depolarization can be attributed to the change in crystal habit at different temperature regimes. Several studies indicate that plate type and hollow column type crystals depolarize less than solid columns (Sassen and Cho, 1992; Takano and Liou, 1995). This suggests that the observed low values of cloud depolarization could be due to the presence of plate type or hollow column type crystals. The difference in the values of cloud depolarization call on geographical differences in the microphysical contents of cirrus clouds, dissimilarities in the formation mechanism and the nature and source of cloud particle forming nuclei, which affect ice crystal shape (Sassen, 1999; Sassen and Takano, 2000). At temperatures lower than −40°C, substantially more large crystals have been observed in tropical cirrus (McFarquhar and Heymsfield, 1997). Heymsfield and MacFarquhar (2002) have shown that while the larger size particle often exceed 1 mm in length for temperatures >-40°C, it decreases to $<100\,\mu$m at temperatures below −60°C. Even though larger particles can exist at higher temperatures the majority of these particles will be more regular in shape with rounded edges. But as temperatures decrease the particles become more irregular in shape with sharper edges. As a result the depolarization increases. The sharp dip in cloud depolarization below −75°C suggests that the particle dimension becomes extremely small at these temperatures. A high population of horizontally oriented plates display near-zero δ values if the lidar was pointed at or very close to the zenith direction (Platt, 1978; Platt et al., 1978). However, since in-situ observations on the change in particle habit below −70°C are not available, the exact mechanism responsible for this dip cannot be conclusively stated at the moment.

4 Summary

This study reveals different forms of cirrus manifestation prevailing over the tropics which can broadly be classified under two types: (a) thin cirrus (laminar) and (b) dense and highly structured cirrus. The most preferred altitude for the formation of tropical cirrus is found to be around 14–16 km. Physical and optical properties of these clouds show significant short-term temporal variations. While on 47% of the nights the cloud continues to persist in the same category throughout the night with a small amount of temporal variation in optical depth, on the remaining nights the variation in cloud optical depth is so large that the cloud type changes from one class to another in short time scales. Most of the sub-visual cirrus are generally symmetric. As the optical depth increases, the cloud becomes more asymmetric. The cloud parameters show significant short-term oscillations, along with a long period variation extending over the entire night. On average, the short-term oscillations in τ_c are in opposite phase with those of ξ and δ. The long-term variations in ξ are found to be in-phase with those of δ and in-phase quadrature with those of τ_c. While the short-term variation in δ and τ_c could be due to corresponding changes in the cloud particle orientation, the long period variations could be associated with the growth and decay phases of the cloud. The cloud depolarization shows a pronounced variation along its vertical. It is generally low near the cloud top and cloud base, with relatively large values in the middle. This could be attributed to the prevailing dynamical processes, such as formation at the top, development in the middle and evaporation at the base within the cloud.

Acknowledgements. The National Atmospheric Research Laboratory (NARL) at Gadanki is an autonomous Facility under Department of Space with partial support from Council of Scientific and Industrial Research. The authors are thankful to the technical and scientific staff of NARL for their dedicated efforts in conducting this experimental programme. The authors also thank the anonymous reviewers for their valuable suggestions.

Topical Editor F. D'Andrea thanks two anonymous referees for their help in evaluating this paper.

References

Ansmann, A., Wandinger, U., Riebesell, M., Weitkamp, C., and Michaels, W.: Independent measurement of extinction and backscatter profiles in cirrus clouds by using a combined Raman elastic backscatter lidar, Appl. Opt., 31, 7113–7131, 1992.

Bodhaine, B. A., Wood, B. N., Dutton, E. G., and Slusser, J. R.: On Rayleigh optical depth calculations, J. Atmos. Ocean. Tech., 16, 1854–1861, 1999.

Boehm, M. T. and Verlinde, J.: Stratospheric influence on upper tropospheric tropical cirrus, Geophys. Res. Lett., 27, 3209–3212, 2000.

Cadel, B., Goldfarb, L., Faduilhe, D., Baldy, S., Giraud, V., Keckhut, P., and Rechou, A.: A Sub-tropical cirrus clouds climatology from Reunion Island (21° S, 55° E) lidar data set, Geophys. Res. Lett., 30(3), 1130, doi:10.1029/2002GL016342, 2003.

Comstock, J. M., Ackerman, T. P., and Mace, G. G.: Ground-based lidar and radar remote sensing of tropical cirrus clouds at Nauru Island: Cloud statistics and radiative impacts, J. Geophys. Res., 107(D23), 4714, doi:10.1029/2002JD002203, 2002.

Dessler, A. E., Palm, S. P., Hart, W. D., and Spinhirne, J. D.: Tropoapuse-level thin cirrus coverage revealed by ICEsat/Geoscience Laser Altimeter System, J. Geophys. Res., 111, D08203, doi:10.1029/2005JD006586, 2006.

Fernald, F. G.: Analysis of atmospheric lidar observations: some comments, Appl. Opt., 23, 652–653, 1984.

Fujita, T. T.: Principle of stereoscopic height computations and their applications to stratospheric cirrus over severe thunder storms, J. Meteorol. Soc. Japan, 60, 355–368, 1982.

Gage, K. S., McAfe, J. R., Carter, D. A., Ecklund, W. L., Riddle, A. C., Reid, G. C., and Balsley, B. B.: Long term mean vertical motion over the tropical Pacific: Wind profiling Doppler radar measurements, Science, 254, 1771–1773, 1991.

Goldfarb, L., Keckhut, P., Chanin, M.-L., and Hauchecorne, A.: Cirrus climatological results from lidar measurements at OHP (44° N, 6° E), Geophys. Res. Lett., 28, 1678–1690, 2001.

Guasta, M. D., Morandi, M., Stefanutti, L., Brechet, J., and Piquad, J.: One year of cloud lidar data from Dumont d'Urville (Antarctica) 1 General overview of geometrical and optical properties, J. Geophys. Res., 98, 18 575–18 587, 1993.

Gultepe, I. and Starr, D. O'C.: Dynamical structure and turbulence in cirrus clouds: Aircraft observations during FIRE, J. Atmos. Sci., 52, 4159–4182, 1995.

Gultepe, I., Starr, D. O'C., Heymsfield, A. J., Uttal, T., Ackerman, T. P., and Wesphal, D. L.: Dynamical characteristics of cirrus clouds from aircraft and radar observations in micro and meso-γ scales, J. Atmos. Sci., 52, 4060–4078, 1995.

Heymsfield, A. J., McFarquhar, G. M., Collins, W. D., Goldstein, J. A., Valero, F. P. J., Spinhirne, J., Hart, W., and Pilewskie, P.: Cloud properties leading to highly reflective tropical cirrus: Interpretations from CEPEX, TOGA COARE and Kwajalein, Marshall Islands, J. Geophys. Res., 103, 8805–8812, 1998.

Heymsfield, A. J. and McFarquhar, G. M.: Mid-latitude and tropical cirrus-Microphysical properties, in: Cirrus, edited by: Lynch, D., Sassen, K., Starr, D. O., and Stephens, G., Oxford University Press, 78–101, 2002.

Imasu, R. and Iwaska, Y.: Characteristics of cirrus clouds observed by laser radar (lidar) during the spring of 1987 and winter of 1987/88, J. Meteorol. Soc. Japan, 69, 401–411, 1991.

Immler, F., Kruger, K., Tegtmeier, S., Fujiwara, M., Fortuin, P., Verver, G., and Schrems, O.: Cirrus clouds, humidity, and dehydration in the tropical tropopause layer observed at Paramaribo, Suriname (5.8° N, 55.2° W), J. Geophys. Res., 112, D03209, doi:10.1029/2006JD007440, 2007.

Jensen, E. J., Toon, O. B., Pfister, L., and Selkirk, H. B.: Dehydration of the upper troposphere and lower stratosphere by subvisible cirrus clouds near the tropical tropopause, Geophys. Res. Lett., 23, 825–828, 1996a.

Jensen, E. J., Toon, O. B., Selkirk, H. B., Spinhirne, J. D., and Schoeberl, M. R.: On the formation and persistence of subvisible cirrus clouds near the tropical tropopause, J. Geophys. Res., 101, 21 361–21 375, 1996b.

Jensen, E. J., Pfister, l., Ackerman, A. S., and Tabazadeh, A.: A conceptual model of the dehydration of air due to freeze-drying by optically thin laminar cirrus rising slowly across the tropical tropopause, J. Geophys. Res., 106, 17 237–17 252, 2001a.

Jensen, E. J., Toon, O. B., Vay, S. A., Ovavlez, J., May, R., Bui, T. P., Twohy, C. H., Gardrud, B. W., Pueschel, R. F., and Schumann, U.: Prevalence of ice-supersaturated regions in the upper troposphere: Implications for opticallt thin ice cloud formation, J. Geophys. Res., 106, 17 253–17 266, 2001b.

Kinne, S., Ackerman, T. P, Heymsfield, A. J., Valero, F. D. J., Sassen, K. and Spinhirne, J. D.: Cirrus microphysics and radiative transfer, Cloud field study on 28 October 1986, Mon. Weather Rev., 120, 661–684, 1992.

Liu, Z., Voegler, P., and Sugimoto, N.: Simulations of the observation of clouds and aerosols with Experiment Lidar in Space Equipment system, Appl. Opt., 39, 3120–3137, 2000.

Luo, B. P., Peter, Th., Wernli, H., Fueglistaler, S., Wirth, M., Kiemle, C., Flentje, H., Yushkov, V., Khattatov, V., Rudakov, V., Thomas, A., Borrmann, S., Toci, G., Mazzingghi, P., Beuermann, J., Schiller, C., Cairo, F., Don-Francesco, G, Di., Adriani, A., Volk, C. M., Strom, J., Noone, K., Mitev, V., MacKenzie, R. A., Carslaw, K. S., Trautmann, T., Santacesaria, V., and Stefanutii, L.: Ultrathin tropical tropopause clouds (UTTCs): II. Stabilization mechanisms, Atmos. Chem. Phys., 3, 1093–1100, 2003, http://www.atmos-chem-phys.net/3/1093/2003/.

Lynch, D. K.: Subvisual cirrus: what it is and where do you find it, in: Proceedings of Passive Infrared Remote Sensing of Clouds and the Atmosphere Conference, SPIE 1934, edited by: Lynch, D., Orlando, FL, pp. 264–274, 1993.

Mace, G. G., Ackerman, T. P., Minnis, P., and Young, D. F.: Cirrus layer microphysical properties derived from surface-based millimeter radar and infrared interferometer data, J. Geophys. Res., 103, 23 207–23 216, 1998.

Macke, A., Francis, P. N., McFarquhar, G. M., and Kinne, S.: The role of ice particle shapes and size distributions in the single scattering properties of cirrus clouds, J. Atmos. Sci., 55, 2874–2883, 1998.

Massie, S. T., Lowe, P., Tie, X., Hervig, M., Thomas, G., and Russell, J.: Effect of the 1997 El Nino on the distribution of upper tropospheric cirrus, J. Geophys. Res., 105, 22 725–22 741, 2000.

Mather, J. H., Ackerman, T. P., Jensen, M. P., and Clements, W. E.: Characterisation of the atmospheric state and the surface radiation budget at the tropical western Pacific ARM site, Geophys. Res. Lett., 25, 4513–4516, 1998.

McFarquhar, G. M. and Heymsfield, A. J.: Parametrisation of tropical cirrus ice crystal size distributions and implications for radaitive transfer: results from CEPEX, J. Atmos. Sci., 54, 2187–2200, 1997.

McFarquhar, G. M., Heymsfield, A. J., Pinhirne, J., and Hart, B.: Thin and subvisual tropopause tropical cirrus: Observations and Radiative Impacts, J. Atmos. Sci., 57, 1841–1853, 2000.

McNeil, W. R. and Carswell, A. I.: Lidar polarisation studies of the troposphere, Appl. Opt., 14, 2158–2168, 1975.

Mergenthaler, J. L., Roche, A. E., Kumer, J. B., and Ely, G. A.: Cryogenic limb array etalon spectrometer observations of tropical cirrus, J. Geophys. Res., 104, 22 183–22 194, 1999.

Osborn, M. T., Poole, L. R., and Wang Pi-Huan: SAM II and lidar aerosol profile comparisons during AASE, Geophys. Res. Lett., 17, 401–404, 1990.

Pace, G., Cacciani, M., di Sarra, A., Fiocoo, G., and Fua, D.: Lidar observations of equatorial cirrus clouds at Mahe Seychelles, J. Geophys. Res., 108(D8), 4236, doi:10.1029/2002JD002710, 2003.

Parameswaran, K., Sunilkumar, S. V., Krishna Murthy, B. V., Satheesan, K., Bhavanikumar, Y., Krishnaiah, M., and Nair, P. R.: Lidar Observations of cirrus cloud near the tropical tropopause: Temporal variations and association with tropospheric turbulence, Atmos. Res., 69, 29–49, 2003.

Peter, Th., Luo, B. P., Wirth, M., Kiemle, C., Flentje, H., Yushkov, V. A., Rudakov, V., Thomas, A., Borrmann, S., Toci, G., Mazzinghi, P., Beuermann, J., Schiller, C., Cairo, F., Donfrancesco, G. D., Adriani, A., Volk, C. M., Strom, J., Noone, K., Mitev, V., MacKenzie, R. A., Carslaw, K. S., Trautmann, T., Santacesaria, V., and Stefanutti, L.: Ultra tropical tropopause clouds (UTTCs): I. Cloud morphology and occurrence, Atmos. Chem. Phys., 3,

1083–1091, 2003,
http://www.atmos-chem-phys.net/3/1083/2003/.

Pfister, L., Selkirk, H. B., Jensen, E., Schoeberl., M. R., Toon, O. B., Browell, E. V., Grant, W, B., Gary, B., Mahoney, M. J., Bui, T. V., and Hintsa, E.: Aircraft observations of thin cirrus clouds near the tropical tropopause, J. Geophys. Res., 106, 9765–9786, 2001.

Platt, C. M. R., Abshire, N. L., McNice, G. T.: Some microphysical properties of an ice cloud from lidar observation of horizontally oriented crystals, J. Appl. Meteorol., 17, 1220–1224, 1978.

Platt, C. M. R. and Dilley, A. C.: Remote sounding of High Clouds IV: Observed temperature variations in cirrus optical properties, J. Atmos. Sci., 38, 1069–1082, 1981.

Platt, C. M. R.: Lidar and radiometric observations of cirrus clouds, J. Atmos. Sci., 30, 1191–1204, 1973.

Platt, C. M. R.: Lidar backscattering from horizontally oriented ice crystal plates, J. Appl. Meteorol., 17, 482–488, 1978.

Platt, C. M. R., Scott, J. C., and Dilley, A. C.: Remote sounding of High Clouds VI: Optical properties of mid latitude and tropical cirrus, J. Atmos. Sci., 44, 729–747, 1987.

Platt, C. M. R., Young, S. A., Manson, P. J., Patterson, G. R., Marsden, S. C., Austin, R. T., and Churnside, J. H.: The optical properties of equatorial cirrus from observations in the ARM pilot radiation observation experiment, J. Atmos. Sci., 55, 1977–1996, 1998.

Prabhakara, C., Fraser, R. S., Dalu, G., Wu, Man-Li C., and Curran, R. J.: Thin cirrus clouds: Seasonal distribution deduced from Nimbus-4 IRIS, J. Appl. Meteorol., 27, 379–399, 1988.

Rao, P. B., Jain, A. R., Kishore, P., Balamuralidhar, P., Damle, S. H., and Viswanathan, G.: Indian MST radar 1. System description and sample vector wind measurements in ST mode, Radio Sci., 30, 1125–1138, 1995.

Rashke, E.: The international satellite cloud climatology project, ISCCP, and its European regional experiment ICE (International Cirrus Experiment), Atmos. Res., 21, 191–201, 1988.

Reichardt, J., Reichardt, S., Hess, M., and McGee T. J.: Correlations among the optical properties of cirrus-cloud particles: Microphysical interpretation, J. Geophys. Res., 107(D21), 4562, doi:10.1029/2002JD002589., 2002.

Revathy, K., Nair, S. R. P., and Krishna Murthy, B. V.: Deduction of temperature profile from MST radar observations of vertical wind, Geophys. Res. Lett., 23, 285–288, 1996.

Robinson, G. D.: The transport of minor atmospheric constituents between the troposphere and stratosphere, Q. J. Roy. Meteor. Soc., 106, 227–253, 1980.

Rosenfield, J. E., Considine, D. B., Schoeberl, M. R., and Browell, E. V.: The impact of subvisible cirrus clouds near the tropical tropopause on stratospheric water vapour, Geophys. Res. Lett., 25, 1883–1886, 1998.

Rossow, W. B. and Schiffer, R. A.: ISCCP cloud data product, B. Am. Meteorol. Soc., 72, 2–20, 1991.

Sakai, T., Shibata, T., Kwon, S.-A., Kim, Y.-S., Tamura, K., and Iwasaka, Y.: Free tropospheric aerosol backscatter, depolarization ratio and relative humidity measured with the Raman lidar at Nagoya in 1994–1997: contributions of aerosols from the Asian Continent and the Pacific Ocean, Atmos. Environ., 34, 431–442, 2000.

Santacesaria, V., Carla, R., MacKenzie, R. A., Adriani, A., Cairo, F., Didonfrancesco, G., Kiemle, C., Redaelli, G., Beuermann, J., Schiller, C., Peter, Th., Luo, B. P., Wernli, H., Ravegnani, F., Ulanovsky, A., Yushkov, V., Sitnikov, N., Balestri, S., and Stefanutti, L.: Clouds at the tropical tropopause: A case study during the APE-THESEO campaign over the western Indian Ocean, J. Geophys. Res., 108(D2), 4044, doi:10.1029/2002JD002166, 2003.

Sasi, M. N.: A reference atmosphere for the Indian equatorial zone. Ind. J. Rad. Space Phys., 23, 299–312, 1994.

Sassen, K. and Cho, B. S.: Subvisual thin cirrus lidar data set for satellite verification and climatological research, J. Appl. Meteorol., 31, 1275–1285, 1992.

Sassen, K. and Campbell, J. R.: A midlatitude cirrus cloud climatology from the facility for atmospheric remote sensing, Part I: Macrophysical and synoptic properties, J. Atmos. Sci., 58, 481–495, 2001.

Sassen, K., Benson, R. P., and Spinhirne, J. D.: Tropical cirrus cloud properties derived from TOGA/COARE airborne polarization lidar, Geophys. Res. Lett., 27, 673–676, 2000.

Sassen, K.: Cirrus clouds and haloes: A closer look, Opt. Photonic News, 10, 39–42, 1999.

Sassen, K., Griffin, M. K., and Dodd, G. C.: Optical scattering and microphysical properties of subvisual cirrus clouds and climatic implications, J. Appl. Meteorol., 28, 91–98, 1989.

Sassen, K. and Takano, Y.: Parry arc: A polarization lidar, ray tracing, and air craft case study, Appl. Opt., 39, 6738–6745, 2000.

Schmidt, E. O., Alvarez, J. M., Vaughan, M. A., and Wylie, D. P.: A review of subvisual cirrus morphology, in: Proceedings of Passive Infrared Remote Sensing of Clouds and the Atmosphere Conference, SPIE 1934, edited by: Lynch, D., Orlando, FL, pp. 230–239, 1993.

Schmidt, E. O. and Lynch, D. K.: Subvisual cirrus: associations to the dynamic atmosphere and radiative effects, in: Proceedings of Passive Infrared Remote Sensing of Clouds and the Atmosphere Conference III, SPIE 2578, edited by: Lynch, D., Paris, pp. 230–239, 1995.

Seifert, P., Ansmann, A., Muller, D., Wandinger U., Althausen D., Heymsfield, A. J., Massie, S. T., and Schmitt, C.: Cirrus optical properties observed with lidar, radiosonde and satellite over the tropical Indian Ocean during the aerosol-polluted northeast and clean maritime southwest monsoon, J. Geophys. Res., 112, D17205, doi:10.1029/2006JD008352., 2007.

Starr, D. O'C. and Cox, S. K.: Cirrus clouds. Part I: A cirus cloud model, J. Atmos. Sci., 42, 2663–2681, 1985a.

Starr, D. O'C. and Cox, S. K.: Cirrus clouds. Part II: Numerical experiments on the formation and maintenance of cirrus, J. Atmos. Sci., 42, 2682–2694, 1985b.

Starr, D. O'C.: A cirrus cloud experiment: Intensive field observations planned for FIRE, B. Am. Meteorol. Soc., 68, 199–124, 1987.

Sunilkumar, S. V. and Parameswaran, K.: Temperature dependence of tropical cirrus properties and radiative effects, J. Geophys. Res., 110, D13205, doi:10.1029/2004JD005426, 2005.

Sunilkumar, S. V., Parameswaran, K., and Krishna Murthy, B. V.: Lidar Observations of cirrus cloud near the tropical tropopause: General features, Atmos. Res., 66, 203–227, 2003.

Takano, Y. and Liou, K. N.: Radiative transfer in cirrus clouds Part III: Light scattering by irregular ice crystals, J. Atmos. Sci., 52, 818–837, 1995.

Thomas, A., Borrmann, S., Kiemle, C., Cairo, F., Volk, M., Beuer-

mann, J., Lepuchov, B., Santacesaria, V., Matthey, R., Rudakov, V., Yushkov, V., MacKenzie, A. R., and Stefanutti, L.: In situ measurements of background aerosol and subvisible cirrus in the tropical tropopause region, J. Geophys. Res., 107(D24), 4763, doi:10.1029/2001JD001385, 2002.

Thomas, L., Cartwright, J. C., and Wareing, D. P.: Lidar observations of the horizontal orientations of ice crystals in cirrus clouds, Tellus, 42B, 211–216, 1990.

Uthe, E. E. and Russell., P. R.: Lidar observations of tropical high altitude cirrus clouds, in: Radiation in the Atmosphere, edited by: Bolle, H. J., Science Press, Princeton, 242–244, 1977.

Wang, P.-H., McCormick, M. P., Poole, L. R., Chu, W. P., Yue, G. K., Kent, G. S., and Skeens, K. M.: Tropical high cloud characteristics derived from SAGE II extinction measurements, Atmos. Res., 34, 53–83, 1994.

Wang, P.-H., Minnis, P., McCormick, M. P., Kent, G. S., and Skeens, K. M.: A 6 year climatology of cloud occurrence frequency from stratospheric aerosol and Gas Experiment II observations (1985–1990), J. Geophys. Res., 101, 29 407–29 429, 1996.

Whitemann, D. N., Demoz, B., and Wang, Z.: Subtropical cirrus cloud extinction to backscatter ratios measured by Raman Lidar during CAMEX-3, Geophys. Res. Lett., 31, L12105, doi:10.1029/2004GL020003, 2004.

Winker, D. M. and Osborn, M. T.: Preliminary analysis of observations of the pinatobo volcanic plume with polarisation sensitive lidar, Geophys. Res. Lett., 19, 171–174, 1992.

Winker, D. M. and Trepte, C. R.: Laminar cirrus observed near the tropical tropopause by LITE, Geophys. Res. Lett., 25, 3351–3354, 1998.

Woodbury, G. E. and McCormick, M. P.: Global distribution of cirrus clouds determined from SAGE data, Geophys. Res. Lett., 10, 1080–1183, 1983.

Wylie, D. P. and Menzel, W. P.: Eight years of high cloud statistics using HIRS, J. Climate, 12, 170–184, 1999.